Food & Function

ROYAL SOCIETY OF CHEMISTRY

PAPER

View Article Online
View Journal | View Issue

Cite this: *Food Funct.*, 2025, **16**, 9033

Flavonoids from *Rosa roxburghii* Tratt fermentation broth inhibit adipogenesis *via* the SIRT1 pathway: insights from metabolomics and network pharmacology

Mi Liu, †[a,c] Youjing Ruan, †[b] Changyudong Huang,[c] Shuang Wang,[d] Yinxue Zhong,[e] Yiyi Zhang,[b] Yongjie Xu*[a,f] and Wei Pan*[a,b,c]

This study explored the metabolic shifts in *Rosa roxburghii* Tratt juice (RRTJ) following fermentation and assessed its impact on adipocyte differentiation. Non-targeted metabolomics revealed significant changes, particularly in flavor-related compounds and flavonoid profiles, with KEGG enrichment analysis highlighting energy metabolism and secondary metabolic pathways. Cluster analysis categorized differentially expressed metabolites into flavor-forming and anti-inflammatory/antioxidant groups. Quantitatively, RRT extract had a flavonoid content of 7.64% (0.764 mg mL^{-1}), while RRTJ and *Rosa roxburghii* Tratt fermentation broth (RRTFB) contained 1.31% and 1.13% flavonoids, respectively. Network pharmacology identified nine key anti-inflammatory/antioxidant compounds, four of which were flavonoids, with molecular docking confirming strong binding affinities to SIRT1. *In vitro* experiments using 3T3-L1 cells demonstrated that RRT-derived flavonoids inhibited adipocyte differentiation by regulating SIRT1 expression. RRT-derived flavonoids exert anti-adipogenic effects *via* SIRT1 pathway activation, offering insights into its functional properties and processing applications.

Received 7th July 2025,
Accepted 17th October 2025

DOI: 10.1039/d5fo02814k

rsc.li/food-function

1. Introduction

Rosa roxburghii Tratt (RRT), a fruit-bearing species of the Rosaceae family, is extensively distributed across the karst mountainous regions of Guizhou, Yunnan, Sichuan, and other provinces in southwestern China.[1] The fruit is distinguished by its exceptionally high ascorbic acid concentration, measuring 2858 mg per 100 grams of fresh weight.[2,3] This concentration is approximately an order of magnitude greater than that observed in kiwifruit and three orders of magnitude higher than that in citrus fruits, thereby warranting its designation as "the King of Vitamin C".[2,3] The key bioactive components in the fruit of RRT include high levels of vitamin C, vitamin P (rutin), superoxide dismutase (SOD), polyphenols, flavonoid compounds, polysaccharides, and organic acids. These constituents collectively endow RRT fruit with a range of physiological regulatory functions: vitamin C and SOD significantly enhance antioxidant capacity by scavenging free radicals and forming an antioxidant defense system; rutin and polysaccharides exert anti-inflammatory and immunomodulatory effects by inhibiting pro-inflammatory factors and enhancing immune cell function; polyphenols and flavonoids synergistically improve metabolic health by regulating lipid metabolism and reducing blood glucose levels; polysaccharides also demonstrate anticancer activity by inhibiting tumor cell metastasis enzyme activity. The integrated actions of these bioactive components render RRT fruit a natural resource rich in nutritional value and health benefits.[1–4]

The juice of RRT (RRTJ) is a common form of consumption that retains the nutritional components of RRT and is easily absorbed. RRTJ exhibits a mildly sour and astringent flavor attributed to its elevated levels of polyphenols and organic acids. These characteristics somewhat restrict its direct consumption and limit its broader market appeal. This limitation can be alleviated through the process of fermentation. During fermentation, microorganisms utilize plant-derived nutrients, such as sugars, for metabolic activities, yielding alcohol, carbon dioxide, and a variety of flavor compounds.[5]

[a]*Prenatal Diagnosis Center, Affiliated Hospital of Guizhou Medical University, Guiyang, 550004, China. E-mail: 313831139@qq.com*
[b]*School of Clinical Laboratory Science, Guizhou Medical University, Guiyang, 550004, China*
[c]*School of Public Health, the Key Laboratory of Environmental Pollution Monitoring and Disease, Control, Ministry of Education, Guizhou Medical University, Guiyang 550025, China*
[d]*Guizhou Branch of Shanghai Children's Medical Center Shanghai Jiaotong University School of Medicine, Guiyang, 550081, China*
[e]*Department of Pathology, Affiliated Hospital of Guizhou Medical University, Guiyang, 550004, China*
[f]*Reproductive Center, Affiliated Hospital of Guizhou Medical University, Guiyang, 550004, China*
†These authors contributed equally to this work.

Simultaneously, microorganisms facilitate the decomposition and transformation of food constituents, such as polyphenols and organic acids.[6] After fermentation, the acidity and astringency of the fruit are significantly reduced, leading to an enhanced palatability. Simultaneously, this process generates unique flavors derived from fermentation, thereby enhancing the product's marketability. Prior studies have indicated that during the fermentation of RRT fruit wine, an extended fermentation period results in a gradual reduction in the fruit's organic acid content and a progressive increase in alcohol content, culminating in a smoother and more refined flavor profile.[6,7]

Commonly employed fermentation techniques include natural and artificial methods. Natural fermentation relies on the inherent microbial community within plants, which is characterized by a stable ensemble of microorganisms capable of self-regulation without the need for external manipulation.[8] Microorganisms' environmental adaptation leads to the formation of region-specific strains, which results in naturally fermented products from different regions exhibiting unique flavors and region-specific bioactive compounds.

In addition to altering flavor profiles, fermented foods enhance nutrient absorption within the body, with certain nutritional benefits being significantly improved. Research suggests that fermented foods are more effective for weight loss compared to their non-fermented counterparts.[9–12] Prior research conducted by our team has demonstrated that RRT-fermented broth (RRTFB) exerts a notable impact on weight reduction. This effect is potentially linked to the ability of RRTFB to enhance SIRT1 expression, which in turn may inhibit lipid formation.[13]

Although extensive research has been conducted on the chemical composition of RRT, the metabolic changes in RRTJ following natural fermentation to form RRTFB remain inadequately characterized. The distinct impacts of these metabolic alterations on the bioactivity profiles of RRTJ and RRTFB are also not well understood. Consequently, a meticulous comparative metabolomic analysis of RRTJ and RRTFB is of paramount importance. Therefore, the present study aims to employ plant metabolomics to analyze the dynamic changes in nutritional components and bioactive substances of RRTJ before and after fermentation. Additionally, network pharmacology and molecular docking will be utilized to elucidate the primary bioactive components and their potential mechanisms of action before and after fermentation. Concurrently, the potential impact of these primary bioactive components on adipocyte differentiation before and after fermentation will be explored. The goal is to provide data support for the production and application of RRT.

2. Materials and methods

2.1 RRTJ and RRTFB

The RRTFB and RRTJ utilized in this study were supplied by Guizhou Shanwangguo Rosa roxburghii Health Industry Co., Ltd. All products employed in this research were commercially packaged finished goods, manufactured in accordance with standardized production protocols and quality control measures established by the supplier (lot no. 20230301). RRTJ was derived through the fresh pressing of RRT fruit, whereas RRTFB was produced using a technology that involved a 300-day low-temperature natural fermentation process. Importantly, neither RRTJ nor RRTFB contained any added water or chemical additives.

2.2 High-resolution untargeted metabolomics analysis of RRTFB and RRTJ (LC-MS/MS analysis)

Metabolomics analysis was conducted utilizing an Ultra-High Performance Liquid Chromatography/Quadrupole Time-of-Flight Mass Spectrometry (UHPLC-Q-TOF MS) system. Sample preparation involved extraction with pre-chilled methanol/acetonitrile/water (2 : 2 : 1, v/v), followed by sonication at a low temperature for 30 minutes. Subsequently, samples were incubated at −20 °C for 10 minutes and centrifuged at 14 000*g* for 20 minutes at 4 °C. The resulting supernatants were lyophilized and reconstituted prior to analysis. Chromatographic separation was achieved using an Agilent 1290 Infinity LC system equipped with a C18 column, maintained at 40 °C, with a flow rate of 0.4 mL min^{-1} and an injection volume of 2 μL. Mass spectrometry was performed on an AB Triple TOF 6600 system, employing alternating scanning in both positive and negative ion modes (*m*/*z* 60–1000). The ion source temperature was maintained at 600 °C, with a collision energy of 35 ± 15 eV. Data-dependent acquisition (DDA) was utilized to collect MS/MS spectra within the *m*/*z* range of 25–1000. Raw data were processed using MSDIAL software, and metabolites were identified by applying criteria of mass error (<10 ppm), retention time, and MS/MS spectra matching against a local database. Following normalization to total peak intensity, principal component analysis (PCA) and orthogonal projections to latent structures-discriminant analysis (OPLS-DA) were conducted. Metabolites exhibiting a variable importance in projection (VIP) > 1 and a $P < 0.05$ were identified as differential. These metabolites were further analyzed for pathway annotation using the Kyoto Encyclopedia of Genes and Genomes (KEGG) database. Quality control (QC) samples were employed to ensure data stability throughout the experimental process, which was carried out by Shanghai Applied Protein Technology Co., Ltd.

2.3 Network pharmacology

The two-dimensional structures of each metabolite were obtained from PubChem (https://pubchem.ncbi.nlm.nih.gov/). Subsequently, the SMILES representations of the target metabolites were input into SwissTargetPrediction to identify the corresponding target genes. All target genes associated with the metabolites were consolidated, and those with a probability greater than 20% were selected, with duplicate genes being removed. The drug–ingredient–target network was then constructed using Cytoscape v3.10.11 to facilitate the analysis of interactions between metabolites and their target genes.

2.4 Molecular docking

The three-dimensional structures of essential target proteins were sourced from the RCSB Protein Data Bank (PDB) (https://www.rcsb.org/). The screening parameters were established with a resolution of less than 2.0 Å and a protein length exceeding 200 amino acids. The crystal structures of the target proteins underwent preprocessing using PyMOL software to eliminate metal ions and ligands. Ligand–protein molecular docking was conducted utilizing Autodock4.2 software. Following the establishment of the docking box, calculations were executed using DockVina to derive ligand–protein molecular docking data, which included affinity (kcal mol^{-1}), root-mean-square deviation (RMSD), and the distance from the lower bound of RMSD (dist from rmsd l.b). Finally, the results were visualized through PyMOL software.

2.5 Determination of flavonoid concentration in samples

To prepare the standard curve for flavonoid concentration detection, rutin was used as the standard. The standard solutions were prepared according to Table 3. 1 mL of the sample to be tested was withdrawn, and the standard curve was prepared. 0.5 mL of 5% $NaNO_3$ was added to both the sample and the standard tubes, and they were allowed to stand at room temperature for 6 minutes. 0.3 mL of 10% $Al(NO_3)_3$ was added and allowed to stand at room temperature for 6 minutes. 3 mL of 0.04 g mL^{-1} NaOH was added and diluted with ethanol to a final volume of 10 mL. The mixture was mixed well and allowed to stand at room temperature for 15 minutes. The absorbance at 510 nm was measured. The standard curve was plotted with absorbance on the *y*-axis and rutin concentration on the *x*-axis. By substituting the absorbance of the tested samples into the formula, the concentration of flavonoids in the samples can be calculated.

2.6 Grouping and treatment of cell experiments

In this study, the 3T3-L1 mouse preadipocyte cell line was employed to investigate adipogenic differentiation. The differentiation process was initiated using a "cocktail induction" approach. Initially, 3T3-L1 cells were cultured in a medium specifically designed for this cell line (Procell, Wuhan) for a duration of 24–48 hours. Upon reaching 80–90% confluence, contact inhibition was triggered. Subsequently, the cells were exposed to Induction Medium A, comprising DMEM High Glucose Medium supplemented with 10% fetal bovine serum, 1% penicillin–streptomycin, 10 μg mL^{-1} insulin, 1 μM dexamethasone, and 0.5 μM IBMX, for 72 hours at 37 °C, with one medium change during this period.

Following this, the medium was substituted with Induction Medium B, which consisted of DMEM High Glucose Medium, 10% FBS, 1% penicillin–streptomycin, and 10 μg mL^{-1} insulin. After 48 hours, Induction Medium B was refreshed for an additional 48 hours, after which it was replaced with DMEM Complete Medium (DMEM High Glucose Medium, 10% FBS, and 1% penicillin–streptomycin, which were all purchased from Procell, Wuhan). The medium was subsequently changed every 48 hours. Successful adipogenic differentiation was verified through Oil Red O staining, which revealed the presence of numerous intracellular lipid droplets.

The cells were categorized into five distinct groups: the NC group (normal control group), the HFD group (induced differentiation group), the EX2 group (300 μg mL^{-1} RRT flavonoid extract), the F20 group (20 μM fisetin), and the H20 group (20 μM herbacetin). Herbacetin and fisetin were purchased as reference standards from Shanghai Yuanye Bio-Technology Co., Ltd. The flavonoid extract was derived from the fruits of *Rosa roxburghii* Tratt., provided by Shanxi SenYuan Bio-Tech Co., Ltd, through standardized extraction and purification processes to selectively enrich active flavonoids while preserving their native bioactive structures. The final product was analytically validated by UV spectrophotometry and HPLC for quantified flavonoid content, meeting phytopharmaceutical standards. Prior to interventions, 3T3-L1 cells were cultured for 48 hours, followed by treatment with gradient concentrations of the extract (100–500 μg mL^{-1}), fisetin (5–100 μM), or herbacetin (5–100 μM). Cell viability was assessed *via* CCK-8 assays at 24 and 48 hours to determine EC_{50} values, which were 442.0/398.4 μg mL^{-1} (extract), 48.14/25.83 μM (fisetin), and 45.62/30.17 μM (herbacetin), respectively. Based on these results, the study employed 300 μg mL^{-1} extract (EX2 group) and 20 μM fisetin (F20) or herbacetin (H20) for subsequent experiments (Fig. S4). Drug interventions (EX2, F20, and H20) were added to both Induction Media A and B during adipogenic differentiation of 3T3-L1 cells to evaluate regulatory effects on lipid accumulation. The HFD group underwent standard differentiation protocols, while the NC group was maintained in DMEM complete medium throughout.

2.7 Oil Red O staining (12-well plate)

Upon completion of adipogenic induction, the cell culture medium was meticulously aspirated. Subsequently, the cells were rinsed with phosphate-buffered saline (PBS), followed by aspiration of the PBS. 200 μL of staining wash solution was introduced along the wall of the well, allowing it to wash for 20 seconds before aspirating the solution. Thereafter, 200 μL of Oil Red O working staining solution was applied and incubated in the dark for 20 minutes. Following incubation, the cells were washed 2–3 times with 500 μL of PBS. Finally, the results were observed and documented using an inverted microscope.

2.8 Analysis of the activation effect of RRT-derived flavonoid extract on SIRT1

The 3T3-L1 cells were exposed to 200 μM of the SIRT1 inhibitor EX527 (Y239843, Beyotime Institute of Biotechnology, Shanghai, China) for a duration of 24 hours to suppress SIRT1 activity. Following this inhibition, the cells were allocated into four distinct experimental groups: the EX527 group (maintained in the DMEM complete medium), the EX2 group (cultured in the DMEM complete medium supplemented with 300 μg mL^{-1} RRT flavonoid extract), the F20 group (cultured in the DMEM complete medium with the addition of 20 μM

fisetin), and the H20 group (cultured in the DMEM complete medium containing 20 μM herbacetin). These groups were maintained for an additional 24 hours, after which the cells were collected for further analysis. Concurrently, a negative control group (NC) was established, wherein no inhibitor was introduced, and the 3T3-L1 cells were cultured solely in the DMEM complete medium.

2.9 Western blotting

Proteins were extracted from 3T3-L1 preadipocytes and subsequently separated using 10% sodium dodecyl sulfate polyacrylamide gel electrophoresis (SDS-PAGE). The resolved proteins were transferred onto polyvinylidene fluoride (PVDF) membranes, which were then incubated overnight at 4 °C with an anti-SIRT1 primary antibody (13161-1-AP, Proteintech, Wuhan, China). Following incubation, the membranes were subjected to washing and developed using an enhanced chemiluminescence (ECL) substrate. Imaging was conducted with a western blot imaging system (Bio-Rad, CA, USA). The gray values of the proteins were quantified using ImageJ software (National Institutes of Health, USA), and the relative expression levels of the target proteins were determined according to the software's protocol. β-Actin served as the reference protein.

2.10 RT-PCR assay (6-well plate)

Total RNA was isolated from the cells of each experimental group utilizing the Total RNA Extractor (B511311-0100, Sangon Biotech, Shanghai, China). The concentration and purity of the RNA were assessed with a Nanodrop 2000 spectrophotometer (Thermo Fisher Scientific, USA). Complementary DNA (cDNA) synthesis was performed using the PrimeScript™ RT reagent kit (RR047A, Takara Bio Inc., Japan). The expression levels of the target genes were quantified through SYBR-Green-based quantitative real-time PCR (qRT-PCR), employing the TB Green™ Premix Ex Taq™ II kit (DRR820A, Takara Bio Inc., Japan).

2.11 Data analysis

Statistical analyses and graphical representations were conducted utilizing GraphPad Prism 9 (GraphPad Software, USA) and Origin 2024 (OriginLab Corporation, USA). The normality of the data was assessed using the Kolmogorov–Smirnov *Z*-test, with normally distributed data expressed as mean ± standard deviation (SD). A one-way analysis of variance (ANOVA) was employed to evaluate mean differences among groups, with statistical significance determined at a threshold of $P < 0.05$.

3. Results

3.1 Results of principal component analysis for the overall sample

For the preparation of QC samples, we initially collected 100 μL of the supernatant from each sample extract, which was then pooled to form a master QC sample. Subsequently, this master QC sample was divided into three portions, each containing 150 μL, to create three QC samples. By comparing the total ion chromatograms (TIC) of these QC samples, we observed that the response intensities and retention times of the chromatographic peaks were largely consistent, indicating a minimal level of systematic error (Fig. S1 and S2).

3.2 Results of principal component analysis for the overall sample

In this study, Principal Component Analysis (PCA) was employed to conduct dimensionality reduction and visualization on the sample data. The PCA results demonstrated that the quality control (QC) samples clustered closely in both positive and negative ionization modes, suggesting that the analytical methods utilized in the experiment exhibited high repeatability and stability. Consequently, the experimental data were deemed reliable, as illustrated in Fig. 1A and B.

3.3 Untargeted plant metabolomics analysis of compositional differences between RRTJ and RRTFB

Upon integrating the detection results from both positive and negative ion modes, a total of 738 valid compounds were identified, with 499 compounds detected in the positive ion mode and 239 in the negative ion mode. Classification analysis revealed that, in the positive ion mode, the predominant compounds were prenol lipids (15.6%), organic oxygen compounds (7.80%), benzene and substituted derivatives (6.00%), fatty acyls (6.00%), carboxylic acids and derivatives (4.80%), and flavonoids (4.40%), among others. In contrast, in the negative ion mode, the main compounds identified were fatty acyls (18.83%), flavonoids (17.15%), prenol lipids (12.13%), benzene and substituted derivatives (9.21%), and organic oxygen compounds (8.37%), among others. Following the integration of both ion modes, the top five compounds in terms of relative abundance were prenol lipids (14.48%), fatty acyls (10.15%), flavonoids (8.53%), organic oxygen compounds (7.98%), and benzene and substituted derivatives (7.04%) (Fig. 1C).

3.4 Differential compound analysis of RRTFB and RRTJ

Utilizing a significance threshold of $P < 0.05$ and a fold change criterion of ≥ 2 or ≤ 0.5, a total of 371 differential compounds were identified in the positive ion mode. Relative to RRTJ, 146 compounds exhibited upregulation, while 225 compounds were downregulated in the RRTFB. In the negative ion mode, 241 differential compounds were detected, comprising 121 upregulated and 120 downregulated compounds in RRTFB as compared to RRTJ (Fig. 1D and E).

Based on partial least squares discriminant analysis (PLS-DA), using VIP > 1 and $P < 0.05$ as criteria, 55 differential compounds were identified in the positive ion mode. Compared to RRTJ, 22 compounds were upregulated and 33 were downregulated in RRTFB. In the negative ion mode, 13 compounds were upregulated and 14 were downregulated in RRTFB relative to RRTJ (Fig. 2A). Among these, compounds with increased levels included metabolites associated with anti-inflammatory, antioxidant, and lipid-lowering activities, such as acetylcholine (POS_581), vanillic acid (NEG_2041), and

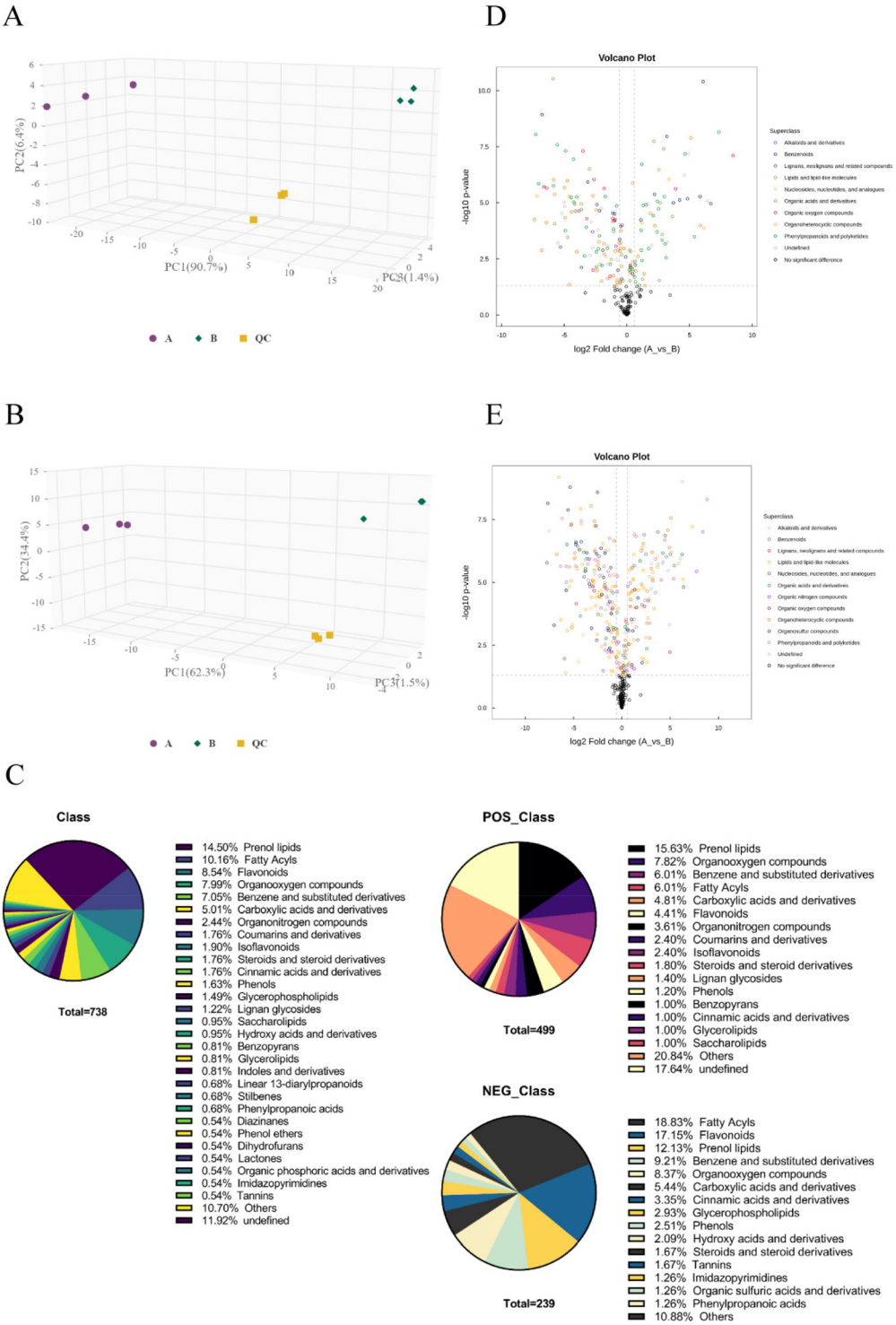

Fig. 1 Metabolite composition analysis of RRTJ and RRTFB. (A) PCA results under negative ion mode. (B) PCA results under positive ion mode. (C) Volcano plot of differential metabolites under negative ion mode (the RRTFB group *vs.* the RRTJ group). (D) Volcano plot of differential metabolites under positive ion mode (the RRTFB group *vs.* the RRTJ group). (E) Pie chart of metabolite classification in RRT.

schisandric acid (POS_3228), as well as food flavor-related compounds like δ-decalactone (POS_1968) and phenyl benzoate (POS_471). Compounds with decreased levels included various carbohydrates such as D-glucose (POS_5318), D-glucosamine (POS_1177), sucrose (NEG_11992), and fructose (NEG_1668), as well as organic acids related to energy metabolism, including ascorbic acid (NEG_1565), *cis*-aconitic acid (POS_306), and L-malic acid (NEG_730) (Fig. 2B).

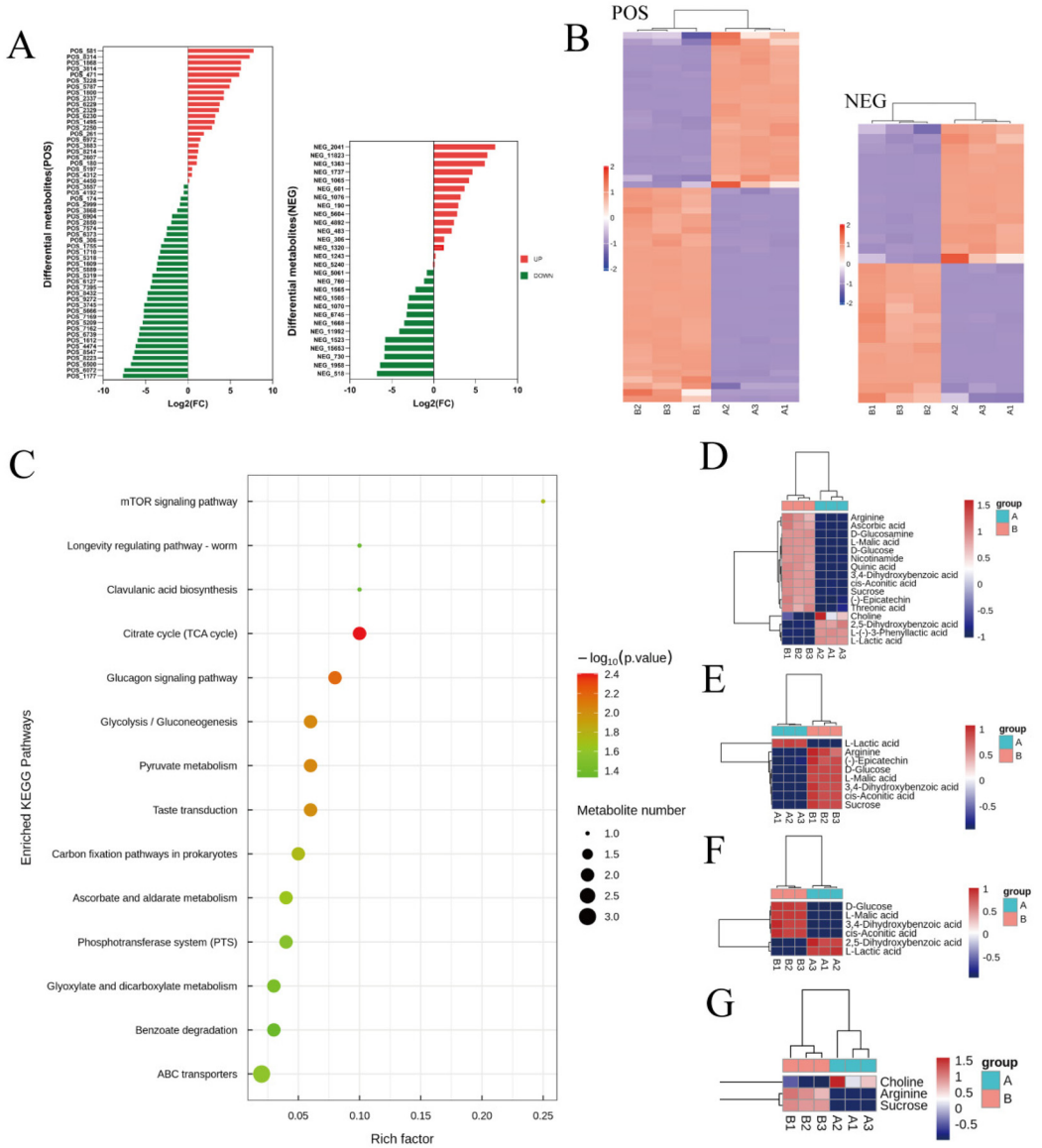

Fig. 2 Differential metabolite analysis of RRTJ and RRTFB (A) analysis of differential metabolites between RRTFB and RRTJ. (B) Heat map of differential metabolites between RRTFB and RRTJ. (C) The KEGG analysis chart of differential metabolites in RRTFB. (D) KEGG analysis of the KO01100 pathway. (E) KEGG analysis of the KO01110 pathway. (F) KEGG analysis of the KO01120 pathway. (G) KEGG analysis of the KO02010 pathway.

3.5 KEGG enrichment analysis

The enrichment analysis utilizing the KEGG metabolic pathway database revealed that the biological functions of compounds in RRTFB demonstrated a significant preference for specific pathways. The differential compounds involved were predominantly metabolites with elevated levels in RRTJ. Employing the hypergeometric distribution test ($P < 0.05$), we identified significantly enriched metabolic pathways that are primarily associated with key biological processes, including energy metabolism regulation (*e.g.*, citric acid cycle, pyruvate metabolism), stress response (*e.g.*, glucagon signaling pathway), and microbial environmental adaptation metabolism (*e.g.*, ABC transporter system) (Fig. 2C). The four pathways encompassing the greatest number of compounds were KO01100 (metabolic pathways), KO01110 (biosynthesis of secondary metabolites), KO01120 (microbial metabolism in diverse environments), and KO02010 (ABC transporters) (Fig. 2D–G). Notably, KO01100 (metabolic pathways) serves as a fundamental metabolic hub, extensively involved in the synthesis and decomposition of primary metabolites such as carbohydrates, amino acids, and lipids, thereby maintaining energy and material homeostasis within organisms. The KO01110 pathway, concerning the biosynthesis of secondary metabolites, emphasizes the production of secondary metabolites such as terpenoids, phenolic acids, and alkaloids, which are crucial for plant defense mechanisms and environmental adaptation. The KO01120 pathway, related to microbial metab-

olism in diverse environments, illustrates the capacity of microbes to adapt to environmental changes through metabolic plasticity, a process intricately linked to the carbon–nitrogen cycle facilitated by high-abundance substances in raw juice (RRTJ). Furthermore, the KO02010 pathway, involving ABC transporters, serves as a fundamental transmembrane transport system that regulates the intracellular accumulation and distribution of dominant metabolites in RRTJ *via* ATP-dependent substrate transport mechanisms. Importantly, the compounds that were significantly enriched within these pathways predominantly originated from the high-abundance components of the RRTJ.

3.6 Cluster analysis of differential compounds between RRTFB and RRTJ

To elucidate the effects of differential compounds between RRTFB and RRTJ, we conducted a cluster analysis on the functions of these compounds, as depicted in Fig. 3A and B. The analysis revealed that the differential compounds could be categorized into two primary groups. The first group comprised 18 compounds associated with anti-inflammatory and antioxidant properties. The second group predominantly consisted of intermediates with ambiguous functions and compounds that influence food flavor. This group included metabolites related to food flavor, which increased in RRTFB, such as δ-decalactone (POS_1968) and phenyl benzoate (POS_471). Additionally, it encompassed various carbohydrates that decreased, including D-glucose (POS_5318), D-glucosamine (POS_1177), sucrose (NEG_11992), and fructose (NEG_1668).

Among the 18 compounds identified for their anti-inflammatory and antioxidant properties, the following exhibited an increase in relative retention time in RRTFB: 3-(4-hydroxy-3-methoxyphenyl) propionic acid (NEG_2041), orsellinic acid (NEG_1363), fisetin (NEG_4892), 2,5-dihydroxybenzoic acid (NEG_1065), morin (NEG_5604), loliolide (POS_1495), hydroxytyrosol (NEG_1076), and 2-palmitoylglycerol (POS_4450) (Table 1). Conversely, the compounds that demonstrated a decrease in RRTFB include diphenylphosphinyl radical (POS_1612), sinapoyl malate (POS_1710), 3,4-dihydroxybenzoic acid (NEG_1070), ascorbic acid (NEG_1565), (−)-epicatechin

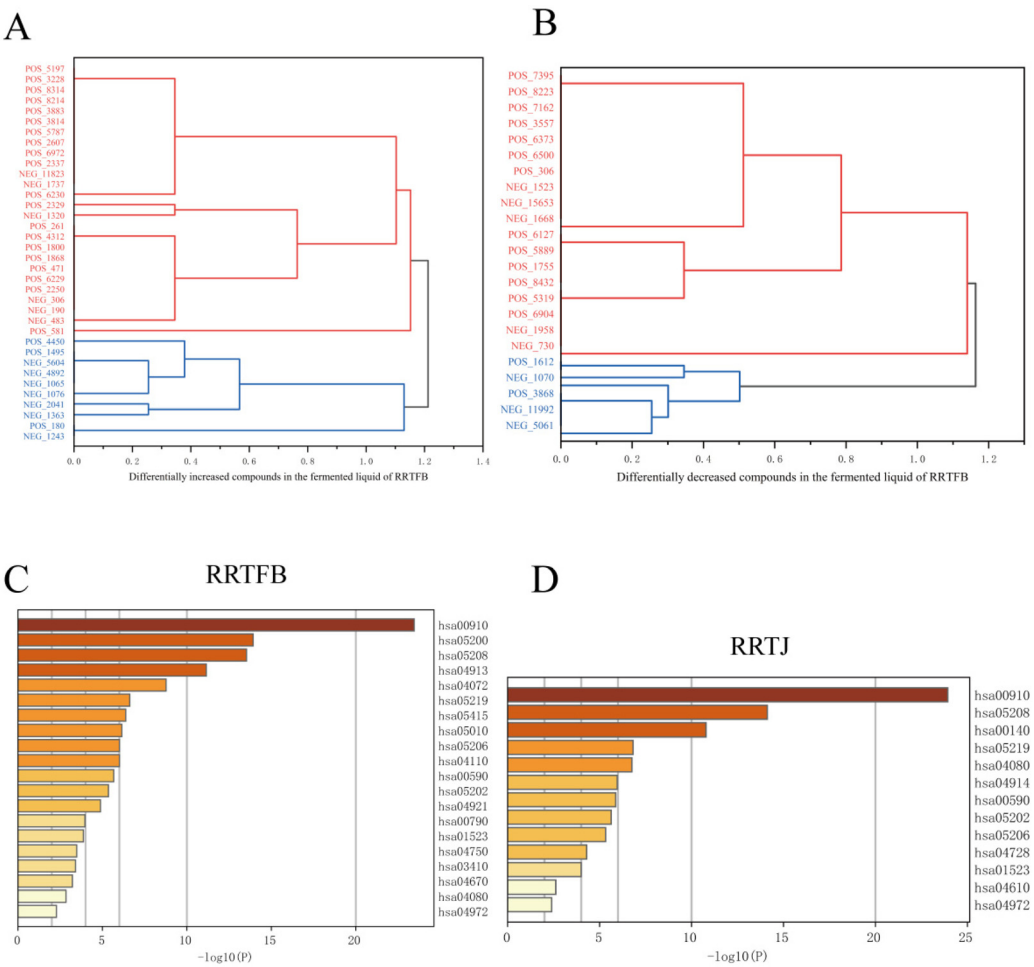

Fig. 3 KEGG enrichment plot (A) differentially decreased compounds in the fermented liquid of RRTFB. (B) Differentially increased compounds in the fermented liquid of RRTFB. (C) KEGG analysis of the anti-inflammatory and antioxidant substances that increase in RRTFB. (D) KEGG analysis of the anti-inflammatory and antioxidant substances that increase in RRTJ.

Table 1 List of elevated differential substances in RRTFB

Identification	Structure types	SMILES	Chemical formula
3-(4-Hydroxy-3-methoxyphenyl) propionic acid	Phenylpropanoids and polyketides	COC1=CC(=CC=C1O)CCC(O)=O	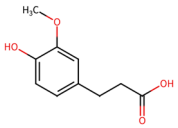
Orsellinic acid	Benzenoids	CC1=C(C(O)=O)C(=CC(=C1)O)O	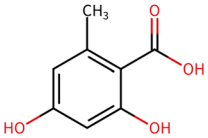
Fisetin	Phenylpropanoids and polyketides	OC1=CC2=C(C=C1)C(=O)C(=C(O2)C3=CC(=C(O)C=C3)O)O	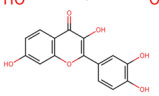
2,5-Dihydroxybenzoic acid	Benzenoids	OC(=O)C1=CC(=CC=C1O)O	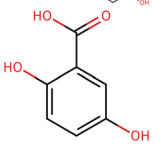
Morin	Phenylpropanoids and polyketides	OC1=CC(=C(C=C1)C2=C(O)C(=O)C3=C(O2)C=C(O)C=C3O)O	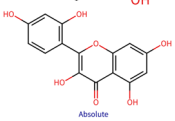
Loliolide	Organoheterocyclic compounds	CC1(C)C[C@H](O)C[C@@]2(C)OC(=O)C=C12	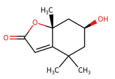
Hydroxytyrosol	Benzenoids	OCCC1=CC=C(O)C(=C1)O	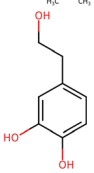
2-Palmitoylglycerol	Lipids and lipid-like molecules	CCCCCCCCCCCCCCCC(=O)OC(CO)CO	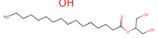

(NEG_5061), hyperoside (NEG_11992), gallic acid hexoside (NEG_6745), herbacetin (POS_3868), gingerol (NEG_5240), and purpurein (POS_7574) (Table 2). A KEGG enrichment analysis of these 18 differential metabolites revealed that they predominantly function through the pathway of chemical carcinogenesis involving reactive oxygen species (hsa05208), which plays a significant role in anti-inflammatory and antioxidant processes (Fig. 3C and D).

3.7 Network pharmacology analysis of major active ingredients in RRTFB and RRTJ

To further elucidate the active components of RRTFB and RRTJ, this study conducted a network pharmacology analysis on 18 differential compounds exhibiting anti-inflammatory and antioxidant properties, along with their corresponding target genes. By selecting target genes with a probability exceeding 20%, nine effective target compounds were identified. These compounds target genes such as the estrogen receptor (ESR1), androgen receptor (AR), aromatase (CYP), SIRT1, and PPAR. Notably, four of the nine compounds are flavonoids: fisetin (NEG_4892), herbacetin (POS_3868), morin (NEG_5604), and hyperoside (NEG_11992). Among these, fisetin and morin demonstrated an increase in RRTFB. Of the remaining five compounds, lecanoric acid (NEG_1363) and 2,5-dihydroxybenzoic acid (NEG_1065) showed an increase in RRTFB (fermented broth), while protocatechuic acid (NEG_1070), gingerol (NEG_5240), and gallic acid hexoside (NEG_6745) exhibited a decrease. Among the flavonoids, fisetin had the highest network contribution degree and ranked first in RRTFB (Fig. 4). In contrast, in RRTJ, herbacetin was the compound with the highest network contribution degree and ranked first (Fig. 4A).

3.8 Molecular docking analysis of the binding interactions between four flavonoid compounds and SIRT1

In prior investigations conducted by our research group utilizing animal models, we observed that the silent information regulator 1 (SIRT1) gene demonstrated a hypermethylated state and reduced expression in cases of obesity. Following the administration of RRTFB, there was a notable upregulation of SIRT1 levels accompanied by a reduction in body weight in the rat subjects. Furthermore, existing studies have indicated that flavonoid compounds possess the capability to modulate SIRT1 expression.[14–16] To examine the potential binding inter-

Table 2 List of reduced differential substances in RRTFB

Identification	Structure types	SMILES	Chemical formula
Diphenylphosphinyl radical	Benzenoids	O=[PH](C1=CC=CC=C1)C2=CC=CC=C2	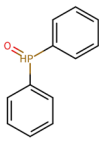
Sinapoyl malate	Phenylpropanoids and polyketides	COC1=C(O)C(=CC(=C1)C=CC(=O)OC(CC(O)=O)C(O)=O)OC	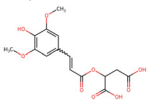
3,4-Dihydroxybenzoic acid	Benzenoids	OC(=O)C1=CC=C(O)C(=C1)O	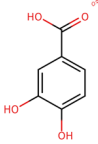
Ascorbic acid	Organoheterocyclic compounds	OCC(O)C1OC(=O)C(=C1O)O	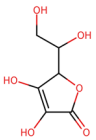
(−)-Epicatechin	Phenylpropanoids and polyketides	OC1CC2=C(OC1C3=CC=C(O)C(=C3)O)C=C(O)C=C2O	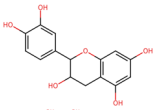
Hyperoside	Phenylpropanoids and polyketides	OCC1OC(OC2=C(OC3=C(C(=CC(=C3)O)O)C2=O)C4=CC(=C(O)C=C4)O)C(O)C(O)C1O	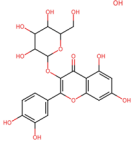
Gallic acid hexoside	Phenylpropanoids and polyketides	OCC1OC(OC(=O)C2=CC(=C(O)C(=C2)O)O)C(O)C(O)C1O	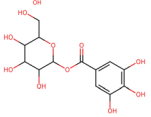
Herbacetin	Phenylpropanoids and polyketides	OC1=CC=C(C=C1)C2=C(O)C(=O)C3=C(O2)C(=C(O)C=C3O)O	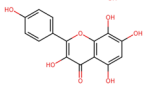
Gingerol	Benzenoids	CCCCC[C@H](O)CC(=O)CCC1=CC(=C(O)C=C1)OC	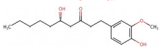
Purpurein	Phenylpropanoids and polyketides	OC[C@H]1O[C@@H](OC2CCCCC2O)[C@H](OC(=O)\\C=C\\C3=CC=C(O)C=C3)[C@@H](O)[C@@H]1O	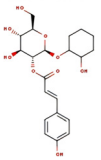

Table 3 Preparation of standard curve for flavonoid concentration determination with rutin standard

Reagents	0	1	2	3	4	5	6
0.2 mg mL^{-1} rutin (mL)	0.00	0.10	0.20	0.40	0.60	0.80	1.00
60% ethanol (mL)	1.00	0.90	0.80	0.60	0.40	0.20	0.00
Final concentration (mg mL^{-1})	0.00	0.02	0.04	0.08	0.12	0.16	0.20

actions between RRT flavonoid (FRT) compounds and SIRT1, this study employed molecular docking techniques utilizing the three-dimensional structure of SIRT1 (PDB ID: 4JSR), which was resolved by X-ray diffraction at a resolution of 1.7 Å. The docking analysis revealed that all four flavonoid molecules demonstrated significant affinity for SIRT1, with binding energies of −14.1 kcal mol^{-1} for fisetin, −14.0 kcal mol^{-1} for morin, −12.1 kcal mol^{-1} for herbacetin, and −8.4 kcal mol^{-1} for hyperoside (Fig. 4B–E).

3.9 Flavonoid content determination

Through network pharmacology screening, we identified that the flavonoids in RRT may exhibit high bioactivity in RRTJ and RRTFB. Consequently, we selected the RRT flavonoid extract and two flavonoid compounds—fisetin and herbacetin—as research subjects. Prior to the study, the flavonoid concentrations in RRTJ, RRTFB, and the RRT flavonoid

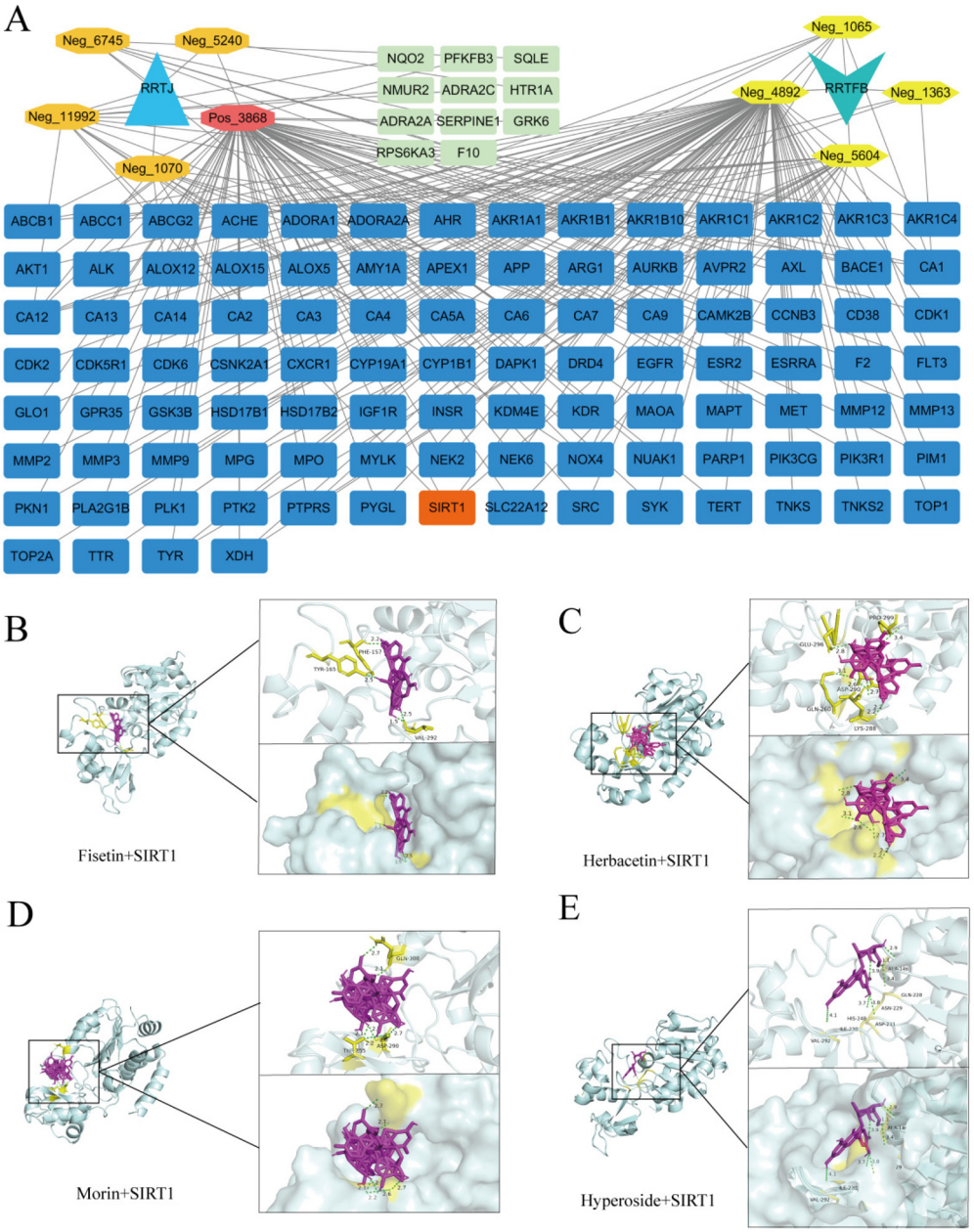

Fig. 4 Network pharmacology and molecular docking diagram. (A) Drug–ingredient–target diagram. Hexagons and octagons represent plant metabolites, while diamonds and rectangles denote genes targeted by metabolites. (B) The molecular docking diagram of fisetin and SIRT1. (C) The molecular docking diagram of herbacetin and SIRT1. (D) The molecular docking diagram of morin and SIRT1. (E) The molecular docking diagram of hyperoside and SIRT1. The purple color in the molecular docking diagram represents small molecule compounds, the pale cyan color represents the protein structure of SIRT1, the numerical value in the right figure represents hydrogen bonding strength, the yellow color represents the binding site between small molecules and proteins, and the amino acids that bind between small molecules and proteins are marked in the small figure above.

extract were analyzed. Rutin contains a 4-carbonyl group with a 3-hydroxyl group or a 4-carbonyl group with a 5-hydroxyl group, a structure that fully meets the standard configuration of flavonoids and plays a critical role in the colorimetric reaction with aluminum ions. Given its structural representativeness, rutin serves as a proxy for the conjugated system of flavonoids, ensuring greater accuracy in total flavonoid quantification. The RRT extract was prepared at a concentration of 10 mg mL^{-1}, and rutin was used as the standard. A standard curve was plotted with concentration as the x-axis and absorbance as the y-axis (Fig. S3). Based on the curve, the total flavonoid concentration in the 10 mg mL^{-1} RRT extract was calculated as 0.764 mg mL^{-1}, corresponding to a flavonoid content of 7.64%. Similarly, the flavonoid contents in RRTJ and RRTFB were determined to be 1.31% and 1.13%, respectively.

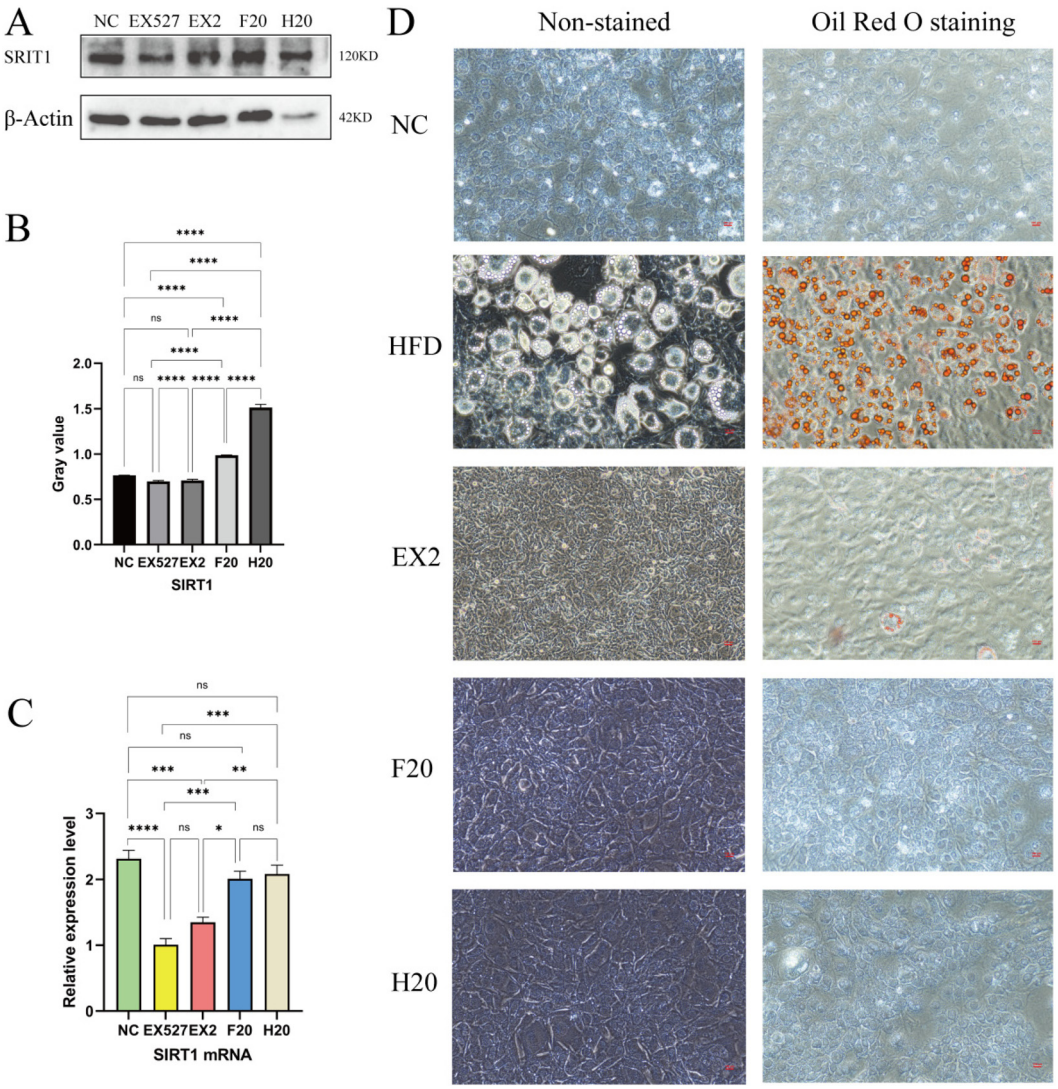

Fig. 5 Effects of FRT on SIRT1 activation and adipogenesis in 3T3-L1 cells. (A) WB analysis bands, with β-actin as the internal reference. (B) Grayscale value analysis results of SIRT1 protein by western blot in 3T3-L1 cells. (C) Detection results of SIRT1 mRNA in 3T3-L1 cells. * $P < 0.05$, ** $P < 0.01$, *** $P < 0.001$, **** $P < 0.0001$. (D) Oil Red O staining results.

3.10 The activation effect of FRT on SIRT1

Numerous phytochemicals function as activators of SIRT1. In this study, molecular docking analysis was employed to predict that flavonoid compounds possess a strong binding affinity for SIRT1. To evaluate the activation effect of FRT on SIRT1, 3T3-L1 cells were initially treated with the SIRT1 inhibitor EX527, followed by FRT intervention. Subsequently, the expression levels of SIRT1 and its downstream targets were assessed. The findings indicated a significant reduction in SIRT1 expression in the EX527 group. Post-intervention, SIRT1 expression was notably upregulated in the F20 and H20 groups ($P < 0.0001$), surpassing levels observed in the NC group ($P < 0.001$). Although SIRT1 levels in the EX2 group were also elevated, the difference was not statistically significant compared to the HFD group (Fig. 5A and B). Additionally, RT-PCR analysis of the collected cells revealed that post-intervention, SIRT1 mRNA levels were increased in the EX2, F20 and H20 groups. This pattern was consistent with the WB findings (Fig. 5C).

3.11 Effect of FRT on adipogenesis of 3T3-L1 preadipocytes

To further elucidate the impact of FRT on adipogenesis, this study utilized cell-based assays for comprehensive analysis. Following adipogenic induction of 3T3-L1 cells, examination of cell growth under an inverted microscope indicated that the majority of cells in the HFD group exhibited oil droplet-like structures, forming string-of-beads patterns within the cells. Oil Red O staining confirmed that these oil droplet-like structures were stained orange-red. Conversely, in the EX2 group treated with FRT extract, only a limited number of cells underwent adipogenic differentiation, with minimal presence of orange-red oil droplet-like structures as evidenced by Oil Red

O staining. In the groups treated with fisetin or herbacetin (F20 and H20 groups), adipogenic differentiation was markedly inhibited, and cell morphology was comparable to that of the NC group (Fig. 5D). These findings suggest that FRT exerts an inhibitory effect on the adipogenic differentiation of 3T3-L1 cells.

3.12 Changes in SIRT1 expression levels during adipogenesis and the interventional effect of FRT

To ascertain whether FRT suppresses adipocyte differentiation through the upregulation of SIRT1 expression, the levels of SIRT1 in 3T3-L1 cells post-induction were evaluated.

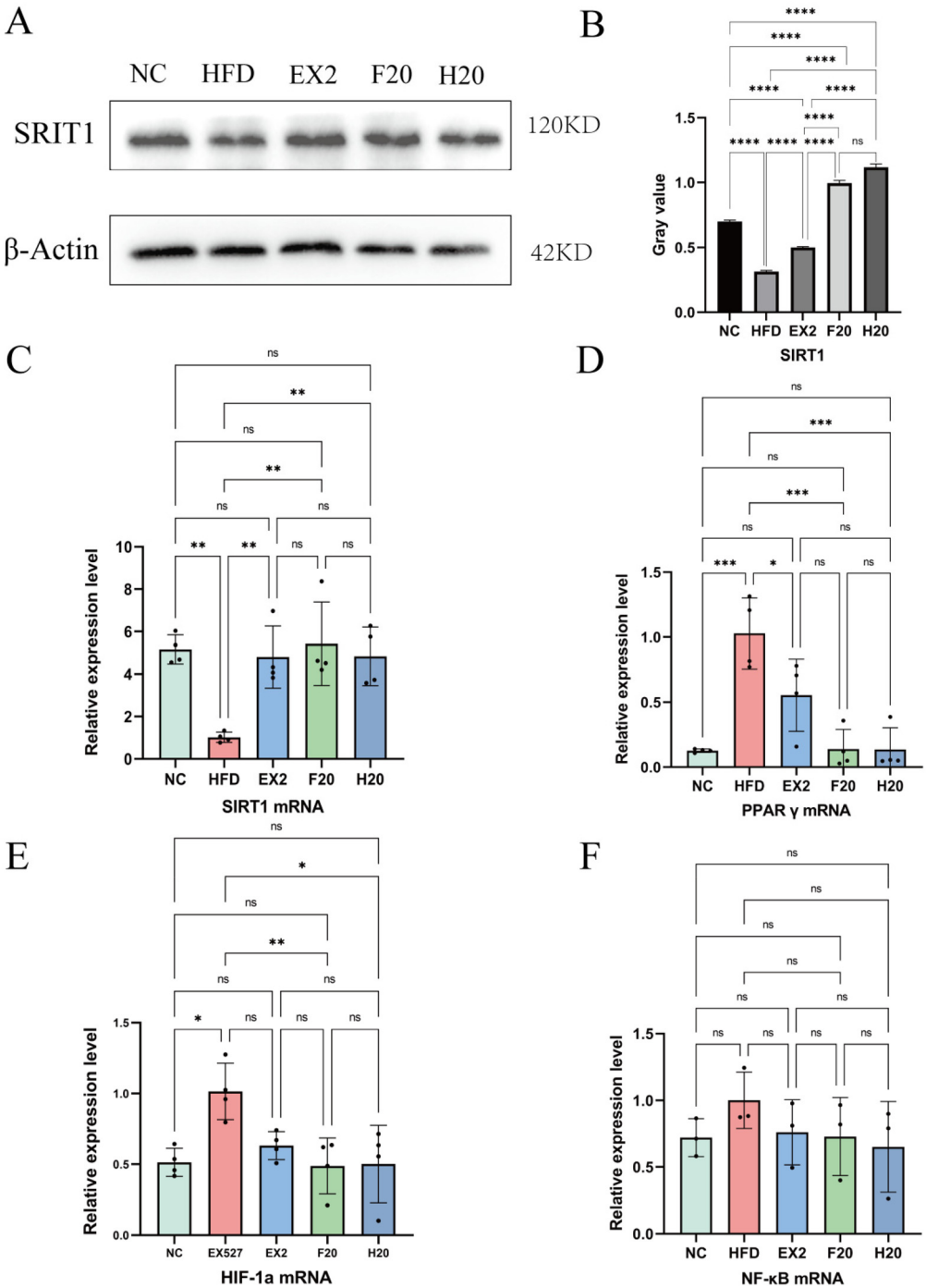

Fig. 6 mRNA expression of SIRT1 and its downstream molecules in cells. (A) WB analysis bands, with β-actin as the internal reference. (B) Grayscale value analysis results of SIRT1 protein by western blot in 3T3-L1 cells. (C) Detection results of SIRT1 mRNA in 3T3-L1 cells. (D) Detection results of PPARγ mRNA in 3T3-L1 cells. (E) Detection results of NF-κB mRNA in 3T3-L1 cells. (F) Detection results of HIF-1α mRNA in 3T3-L1 cells.

Quantitative RT-PCR was employed to quantify the mRNA levels of SIRT1 and its downstream molecules. The findings revealed that (Fig. 6A–C), in comparison with the HFD group, the F20 and EX2 groups exhibited a significant upregulation of SIRT1 expression ($P < 0.001$). Furthermore, all drug-treated groups demonstrated a significant reduction in the expression levels of PPARγ, NF-κB, and HIF-1α ($P < 0.05$) (Fig. 6D–F).

4. Discussion

RRT is a medicinal and edible plant characterized by its rich nutrient profile. Employing UHPLC-QTOF-MS, researchers conducted an analysis of the essential oil derived from *Rosa roxburghii*. This analysis led to the identification of 59 compounds, comprising 13 organic acids, 12 flavonoids, 11 terpenoids, 9 amino acids, and 5 phenylpropanoid derivatives, among others.[17] In this study, by employing a non-targeted metabolomics approach, a total of 738 compounds were identified in RRTJ, both before and after natural fermentation. The analysis highlighted a significant abundance of prenol lipids, fatty acyls, and flavonoids among the detected compounds.

4.1 The metabolite composition of RRTJ underwent alterations as a result of the fermentation process

After fermentation, differential metabolites were predominantly enriched in carbohydrates, organic acids, and compounds with anti-inflammatory and antioxidant properties. Notably, the concentrations of carbohydrates, including glucose and fructose, showed a significant decrease, which is consistent with the characteristic microbial utilization of these sugars for metabolic processes. Concurrently, the levels of organic acids, such as ascorbic acid and malic acid, also decreased, possibly due to microbial decomposition of these acids or their conversion into other flavor compounds during fermentation. This finding elucidates the observed reduction in sourness and astringency in RRTFB.[18–20] Furthermore, the emergence of flavor-related compounds, such as δ-decalactone and phenyl benzoate, significantly enhanced the taste profile of RRTFB. This observation is in agreement with the existing literature, which highlights the optimization of food flavor and functional components through fermentation processes.[21,22]

It is noteworthy that the anti-inflammatory and antioxidant-related metabolites in the fermentation broth exhibited a pattern of "partial increase and partial decrease" relative to the original liquid. Specifically, the concentrations of flavonoids, such as fisetin and morin, were markedly increased, while those of herbacetin and hyperoside were decreased. This variation could be ascribed to microbial structural modifications, including glycoside hydrolysis, or the degradation of flavonoids during metabolic processes.[23,24] KEGG enrichment analysis revealed that the differential metabolites were predominantly associated with energy metabolism pathways, such as the citric acid cycle (also known as the Krebs cycle or TCA cycle) and pyruvate metabolism, as well as pathways involved in the biosynthesis of secondary metabolites. This suggests that fermentation may enhance the production of antioxidant and anti-inflammatory compounds by altering carbon and nitrogen metabolism pathways. Notably, alterations in the flavonoid content of RRTFB were particularly significant. For instance, the concentration of fisetin, a natural antioxidant, was markedly elevated in RRTFB. Fisetin has been demonstrated to exert anti-inflammatory effects by scavenging free radicals and modulating inflammatory cytokines.[25–28] The study's findings indicate that fermentation not only enhances the sensory profile of RRTJ by improving its taste and aroma but also boosts its functional properties through metabolic reprogramming. Despite the observed decrease in ascorbic acid levels following fermentation, which could potentially reduce the antioxidant potential of RRTJ, the concurrent emergence of flavonoids and phenolic acids during fermentation may counterbalance this effect through synergistic actions. This possibility merits further exploration.

4.2 FRT inhibit adipogenesis *via* the SIRT1 pathway

This study, employing network pharmacology and molecular docking analyses, demonstrated that flavonoid-rich therapies (FRT), including compounds such as fisetin and herbacetin, exhibit effective binding to the SIRT1 protein. The binding energies observed, ranging from −8.4 to −14.1 kcal mol^{-1}, suggest a high binding affinity. Flavonoids, characterized by their polyphenolic nature and 2-phenylchromone core structure, possess phenolic hydroxyl groups capable of donating hydrogen atoms to peroxyl radicals. This donation results in the formation of flavonoid radicals, which subsequently interact with other radicals, thereby interrupting the chain reaction processes of free radicals. Consequently, flavonoids demonstrate significant antioxidant activity.[29] Similar to ascorbic acid, the total flavonoid content in RRT is greater than that found in typical fruits and vegetables.[30]

SIRT1 plays a pivotal role in regulating various processes involved in the remodeling of adipocytes associated with obesity.[31,32] SIRT1 is ubiquitously expressed in various tissues throughout the body, including white adipose tissue, and plays a critical role in enhancing cellular resistance to external stress and improving metabolic processes, among other functions. As an NAD ± dependent deacetylase, it facilitates fatty acid oxidation and suppresses adipogenesis by activating the downstream AMPK/PGC-1α signaling pathway.[33,34] This study corroborated the proposed mechanism through cellular experiments, demonstrating that the flavonoid extract from RRT, including fisetin and herbacetin, inhibited adipogenic differentiation in 3T3-L1 cells while upregulating the expression of SIRT1 protein and mRNA. These findings align with our previous results from animal experiments, suggesting that RRTFB mitigates obesity by activating SIRT1. It is hypothesized that alterations in flavonoid composition during fermentation, such as an increase in fisetin content, may enhance the activation of SIRT1, thereby inhibiting the expression of key adipogenic factors like PPARγ and obstructing the adipocyte differentiation process.

5 Conclusion

In this study, we systematically analyzed the metabolic profile of RRTJ and investigated the impact of natural fermentation on its composition. We found that RRTJ is rich in bioactive flavonoids such as luteolin, which confer its anti-inflammatory and antioxidant properties. The fermentation process slightly adjusted the composition of RRTJ, reducing the content of carbohydrates and organic acids, and increasing the content of specific flavonoids, particularly quercetin, which is more abundant in RRTFB. These flavonoids inhibit adipocyte differentiation by activating the SIRT1 signaling pathway, enhancing the nutritional value and functionality of RRTFB. Our results indicate that both RRTJ and RRTFB exert their lipogenic inhibitory effects through the SIRT1 pathway, further confirming the central role of flavonoids in RRTJ and its fermented products (Fig. S5). This provides new insights into the potential mechanisms by which these products regulate metabolic health and lays the foundation for future research and applications.

Further research should delve into the mechanisms behind the metabolic profile changes during fermentation and their impact on product functionality. Exploring the potential of RRTFB products in preventing obesity and metabolic diseases will provide a scientific basis for developing new health foods. Lastly, assessing the sensory quality and consumer acceptance of fermented RRT products, especially the impact of flavor compound changes on sensory attributes,[35] will guide their application in the food industry.

Author contributions

Mi Liu: conceptualization (equal); data curation (equal), formal analysis, writing – original draft preparation (equal), writing – review and editing (equal), and funding acquisition; Youjing Ruan: software (equal), writing – original draft preparation (equal), methodology (equal), validation (equal), data curation (equal), and writing – review and editing (equal); Chengyudong Huang: methodology (equal) and software (equal); Shuang Wang: methodology (equal) and data curation (equal); Yiyi Zhang: methodology (equal); Yinxue Zhong: methodology (equal); Yongjie Xiu and Wei Pan: conceptualization (equal) and supervision (equal).

Conflicts of interest

The authors declare no conflict of interest.

Data availability

Data are contained within the article and its supplementary information (SI). Supplementary information is available. See DOI: https://doi.org/10.1039/d5fo02814k.

Acknowledgements

This work was carried out with the support of the "Science and Technology Program of Guizhou Provincial (ZK[2023] General 322)" and the "Guizhou Provincial Health Commission Science and Technology Fund Project (gzwkj 2024-227)".

References

1 J. Ji, S. Zhang, M. Yuan, *et al.*, Fermented *Rosa roxburghii* Tratt Juice alleviates high-fat diet-induced hyperlipidemia in rats by modulating gut microbiota and metabolites, *Front. Pharmacol.*, 2022, **13**, 883629.
2 Z. H. Zhu, B. J. Wu, R. B. Zheng, X. D. Huang and J. B. Ye, Analysis of vitamin C in *Rosa roxburghii* and its preserved fruits, *Beverage Ind.*, 2021, **24**(2), 40–44.
3 Y. Y. Yin, J. Zhang, L. W. Lu, L. L. Li and D. Q. Zhang, Research progress on polyphenolic substances in *Rosa roxburghii*, *Food Mach.*, 2024, **40**(1), 234–240.
4 P. H. Wu, S. C. Han and M. H. Wu, Beneficial effects of hydroalcoholic extract from *Rosa roxburghii* Tratt fruit on hyperlipidemia in high-fat-fed rats, *Acta Cardiol. Sin.*, 2020, **36**(2), 148–159.
5 Y. Li, P. Ding, X. Tang, *et al.*, Screening and oenological property analysis of ethanol-tolerant non-*Saccharomyces* yeasts isolated from *Rosa roxburghii* Tratt, *Front. Microbiol.*, 2023, **14**, 1202440.
6 Z. H. Yu, G. D. Huang, X. Y. Huang, *et al.*, A comparative study of yeasts for *Rosa roxburghii* wine fermentation, *Fermentation*, 2022, **8**(7), 311.
7 A. Baharin, T. Y. Ting and H. H. Goh, Post-proline cleaving enzymes (PPCEs): Classification, structure, molecular properties, and applications, *Plants*, 2022, **11**(10), 1330.
8 V. Alessandria, I. Ferrocino, V. Carta, *et al.*, Selection of food cultures with protective properties for cooked ham, *Food Microbiol.*, 2023, **112**, 104218.
9 M. Jalili, M. Nazari and F. Magkos, Fermented foods in the management of obesity: Mechanisms of action and future challenges, *Int. J. Mol. Sci.*, 2023, **24**(3), 2665.
10 P. S. Ares, G. Gaur, B. P. Willing, F. Weber, A. Schieber and M. G. Gänzle, Antibacterial and enzyme inhibitory activities of flavan-3-ol monomers and procyanidin-rich grape seed fractions, *J. Funct. Foods*, 2023, **107**, 105643.
11 S. Shyam, D. C. Greenwood, C. W. Mai, *et al.*, Major dietary patterns in the United Kingdom Women's Cohort Study showed no evidence of prospective association with pancreatic cancer risk, *Nutr. Res.*, 2023, **118**, 41–51.
12 S. K. Walsh, K. Pettigrew, I. Mezzani, *et al.*, Role of selenium and 17β oestradiol in modulating lipid accumulation in in vitro models of obesity and NAFLD, *Food Med. Homol.*, 2025, **2**(4), 9420056.
13 M. Liu, H. Li, J. Zhang, *et al.*, Flavonoids in *Rosa roxburghii* Tratt fermentation broth ameliorate obesity via DNMT3a/SIRT1-mediated epigenetic modulation, *Food Sci. Nutr.*, 2025, **13**(9), e70892.

14 Y. Guo, L. Xing, C. D. Qian, Z. Ding and B. Jin, Involvement of flavonoids from the leaves of *Carya cathayensis* Sarg. in sirtuin 1 expression in HUVEC senescence, *Evidence-based Complementary and Alternative Medicine*, 2018, **2018**, 8246560.

15 A. M. Sayed, E. Hassanein, S. H. Salem, O. E. Hussein and A. M. Mahmoud, Flavonoids-mediated SIRT1 signaling activation in hepatic disorders, *Life Sci.*, 2020, **259**, 118173.

16 F. Zhang, J. Feng, J. Zhang, *et al.*, Quercetin modulates AMPK/SIRT1/NF-κB signaling to inhibit inflammatory/oxidative stress responses in diabetic high fat diet-induced atherosclerosis in the rat carotid artery, *Exp. Ther. Med.*, 2020, **20**(6), 280.

17 M. H. Liu, Q. Zhang, Y. H. Zhang, X. Y. Lu, W. M. Fu and J. Y. He, Chemical analysis of dietary constituents in *Rosa roxburghii* and *Rosa sterilis* fruits, *Molecules*, 2016, **21**(9), 1204.

18 Z. W. Song, H. Du, M. H. Zhang, Y. Nie and Y. Xu, *Schizosaccharomyces pombe* can reduce acetic acid produced by Baijiu spontaneous fermentation microbiota, *Microorganisms*, 2019, **7**(12), 606.

19 R. Duliński, B. Stodolak, Ł. Byczyński, A. Poreda, A. Starzyńska-Janiszewska and K. Żyła, Solid-state fermentation reduces phytic acid level, improves the profile of myo-inositol phosphates and enhances the availability of selected minerals in flaxseed oil cake, *Food Technol. Biotechnol.*, 2017, **55**(3), 413–419.

20 J. Barrios-González and A. Mejía, Production of secondary metabolites by solid-state fermentation, *Biotechnol. Annu. Rev.*, 1996, **2**, 85–121.

21 J. Tang, Y. Liu, B. Lin, *et al.*, Effects of ultra-long fermentation time on the microbial community and flavor components of light-flavor Xiaoqu Baijiu based on fermentation tanks, *World J. Microbiol. Biotechnol.*, 2021, **38**(1), 3.

22 A. Liu, X. Yang, Q. Guo, *et al.*, Microbial communities and flavor compounds during the fermentation of traditional Hong Qu glutinous rice wine, *Foods*, 2022, **11**(8), 1097.

23 M. Ishikawa, M. Kawasaki, Y. Shiono and T. Koseki, A novel *Aspergillus oryzae* diglycosidase that hydrolyzes 6-O-α-L-rhamnosyl-β-D-glucoside from flavonoids, *Appl. Microbiol. Biotechnol.*, 2018, **102**(7), 3193–3201.

24 C. A. Kayath, A. Ibala Zamba, S. N. Mokémiabeka, M. Opa-Iloy, P. S. Elenga Wilson, M. D. Kaya-Ongoto and E. Nguimbi, Synergic involvements of microorganisms in the biomedical increase of polyphenols and flavonoids during the fermentation of ginger juice, *Int. J. Microbiol.*, 2020, **2020**, 8417693.

25 P. Zhang and J. Cui, Neuroprotective effect of fisetin against the cerebral ischemia–reperfusion damage via suppression of oxidative stress and inflammatory parameters, *Inflammation*, 2021, **44**(4), 1490–1506.

26 G. Grynkiewicz and O. M. Demchuk, New perspectives for fisetin, *Front. Chem.*, 2019, **7**, 697.

27 H. H. Park, S. Lee, J. M. Oh, M. S. Lee, K. H. Yoon, B. Y. Park, J. W. Kim, H. Song and S. H. Kim, Anti-inflammatory activity of fisetin in human mast cells (HMC-1), *Pharmacol. Res.*, 2007, **55**(1), 31–37.

28 N. Khan, D. N. Syed, N. Ahmad and H. Mukhtar, Fisetin: a dietary antioxidant for health promotion, *Antioxid. Redox Signaling*, 2013, **19**(2), 151–162.

29 P. W. Barnes, M. A. Tobler, K. Keefover-Ring and S. D. Flint, Rapid modulation of ultraviolet shielding in plants is influenced by solar ultraviolet radiation and linked to alterations in flavonoids, *Plant, Cell Environ.*, 2016, **39**(1), 222–230, DOI: 10.1111/pce.12609.

30 Q. Q. Yang, D. Zhang, A. K. Farha, X. Yang, H. B. Li, K. W. Kong and J. R. Zhang, Phytochemicals, essential oils, and bioactivities of an underutilized wild fruit Cili (*Rosa roxburghii*), *Ind. Crops Prod.*, 2020, **143**, 111928.

31 M. P. Gillum, M. E. Kotas, D. M. Erion, R. Kursawe, P. Chatterjee, K. T. Nead, E. S. Muise, J. J. Hsiao, D. W. Frederick, S. Yonemitsu, A. S. Banks, L Qiang, S. Bhanot, J. M. Olefsky, D. D. Sears, S. Caprio and G. I. Shulman, SirT1 regulates adipose tissue inflammation, *Diabetes*, 2011, **60**(12), 3235–3245.

32 Q. Tang, Z. H. Liang, J. J. Yuan, *et al.*, FER1L6 ameliorates insulin resistance by regulating GLUT4 expression, *Food Med. Homol.*, 2025, **2**(4), 9420070.

33 X. Yang, Q. Liu, Y. Li, Q. Tang, T. Wu, L. Chen, S. Pu, Y. Zhao, G. Zhang, C. Huang, J. Zhang, Z. Zhang, Y. Huang, M. Zou, X. Shi, W. JIang, R. Wang and j. He, The diabetes medication canagliflozin promotes mitochondrial remodelling of adipocyte via the AMPK-Sirt1-Pgc-1α signalling pathway, *Adipocyte*, 2020, **9**(1), 484–494.

34 Y. Majeed, N. Halabi, A. Y. Madani, A. Al-Ali, S. Al-Musawi, H. Al-Salami and S. Al-Musawi, SIRT1 promotes lipid metabolism and mitochondrial biogenesis in adipocytes and coordinates adipogenesis by targeting key enzymatic pathways, *Sci. Rep.*, 2021, **11**(1), 8177.

35 Q.-Y. Hu, X.-X. Tang, Z. Li, *et al.*, Effects of lactic acid bacteria fermentation on antioxidant activity and sensory quality of Rosa sterilis S D Shi, *Food Med. Homol.*, 2025, **2**(1), 9420026.